

Quantum Correlations and Entanglement in Generalized Dicke-Ising Models

Santiago F. Caballero-Benitez^{1*}

¹*Instituto de Física, LSCSC-LANMAC, Universidad Nacional Autónoma de México, Ciudad de México 04510, Mexico*

(Dated: March 17, 2026)

Quantum systems inside high-Q cavities offer an excellent testbed for the control of emergent symmetries induced by light and their interplay with quantum matter. Recently several developments in cavity experiments with neutral atoms and other quantum objects such as ions motivate the study of their quantum correlated properties and their entanglement to tailor and control the behavior of the system. Using the enhanced coupling between light and interacting matter we explore the properties of emergent superradiant modes using our newly developed Light-Matter DMRG algorithm with strongly interacting spin chains. We explore a experimentally viable generalization of the transverse Ising chain coupled to the cavity light where it is possible to induce multimode structures tailored by the light pumped into the system. We find a plethora of scenarios can be explored with clear and accesible measurable signatures. This allows to study the physics of emergent orders and strong quantum correlations with quantum spins where the local and long range coupling can be efficiently simulated. We find that quantum spin nematic states with long range order and magnon pairs emerge as the transitions to superradiant phases take place. Notably, we show the cavity field allows the optimization of entanglement between spins for different light induced modes which can be used for quantum state engineering of quantum correlated states. Our methods can be used to model other hybrid quantum systems efficiently.

Quantum scatterers inside high-Q cavities or confined in waveguides offer a unique opportunity to study how strong light-matter coupling can influence the emergence of macroscopic ordering and how quantum correlations determine the properties of the system. Recent advances in cavity systems with ultracold atoms¹, motivate to explore in other systems such as effective spins, how the properties of the system can be controlled. Using the geometry of light it is possible to induce modes that collectively scatter light in groups across the system²⁻⁴. These groups of quantum objects will have collective emission that can be exploited for quantum information purposes. Moreover, as light matter interaction becomes strong inside the cavity, superradiance (SR) emerges^{5,6} triggering a quantum phase transition⁷ while modifying the collective properties of the scatterers due to cavity back action. Thus, macroscopic order emerges controlled by how we pump light into the system by design. In an array of these emitters, we can have that different macroscopic orders compete similar to atomic systems where several quantum correlated states have been observed, such as insulators and supersolids⁸⁻¹⁰, while magnetic ordering is also possible¹¹⁻¹³. In effective spin systems inside cavities such as neutral atoms¹⁴, Rydberg atoms^{15,16}, ions in wave guides^{17,18} using the motional degrees of freedom and in atoms near waveguides^{19,20}, the situation is similar structurally which motivates our work. With this in mind, we study a prototypical setup to explore the collective properties of interacting spins with its interplay with cavity light in a one dimensional setup. The interaction mediated by the cavity effective couples all the spins in the system with a global structured interaction that competes with the underlying structure that the spins have. The spins in their most simple form can interact with each other as in the Ising model, providing the system

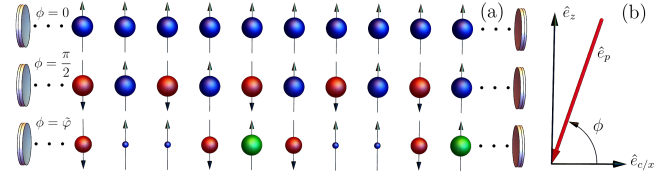


FIG. 1. Light mode structure induced to the spin chains in the cavity (a)-(b), Experimental scheme for the light. Panel (a): Spins along the chain, sphere size is proportional to the light mode coupling strength at each site. The diffraction maxima configuration ($\phi = 0$), a ferromagnetic mode is induced [●●]. The diffraction minima configuration ($\phi = \pi/2$), generates a staggered spin field [●●]. The golden ratio (RBBRG) configuration ($\phi = \arccos(1/5) = \tilde{\varphi}$) inducing a three mode staggered spin structure (red, blue, green) every 5 sites [●●●●●]. The arrows point the direction of the spin in the quantization axis “ x ”. Panel (b): The light setup, the angle ϕ between the cavity axis \hat{e}_c and the light pumped into the system with direction \hat{e}_p ($-\hat{e}_p$) for a standing wave cavity and retro-reflected pump beams in the pump axis from the side (only one is shown, the other one is parallel). The light polarization unit vector is \hat{e}_z and the spins are along the spatial axis \hat{e}_x .

with effectively an anharmonic deformation to the energy structure of the system. The fact that now the system has many body interactions in two fronts via the cavity light and the direct spin interactions will trigger competition of orders akin to the situation in ultracold atomic systems. As a consequence of this, quantum phase transitions emerge and the SR phases can have non-trivial properties. Further, we present a rich landscape of quantum many body phases for the spin ordering with useful

Identifier	Phase	$ \langle \hat{a} \rangle $	\mathcal{M}_0^z	\mathcal{M}_0^x	\mathcal{M}_π^z	\mathcal{M}_π^x	\tilde{Q}^B	$\tilde{\mathcal{P}}$
I	N-FM _z	0	$\neq 0$	0	0	0	0	0
II	N-AFM _z	0	0	0	$\neq 0$	0	0	0
III	SR-FM _x	$\neq 0$	0	$\neq 0$	0	0	≈ 0	$\neq 0$
IV	SR-AFM _x	$\neq 0$	$\neq 0$	0	0	$\neq 0$	≈ 0	$\neq 0$
V	SR-FM _x - \tilde{Q}^B	$\neq 0$	0	$\neq 0$	0	0	$\neq 0$	$\neq 0$
VI	SR-AFM _x - \tilde{Q}^B	$\neq 0$	0	0	0	$\neq 0$	$\neq 0$	$\neq 0$
VII	SR-FM _{φ} - \tilde{Q}^B	$\neq 0$	$\neq 0$	$\neq 0$	≈ 0	≈ 0	$\neq 0$	$\neq 0$

TABLE I. **Quantum phases of the spins and their order parameters.** The order parameters are the amplitude $|\langle \hat{a} \rangle|$ of the light field, the magnetization \mathcal{M}_0^ν , staggered magnetization \mathcal{M}_π^ν , the mean bond nematic order parameter \tilde{Q}^B , the magnon pair order parameter $\tilde{\mathcal{P}}$ and the dominant spin axis $\nu = x/z$. The resulting phases are combinations of normal N or superradiant order R, the dominant spin axis induced by the light and how it is transferred to the spins generating FM/ AFM in “x” or Multimode FM order with golden ratio coupling φ , the bond quadrupolar order in the spins and the emergence of magnon pairs with long range order.

properties in the structures seeded by light for quantum information purposes as the entanglement can be controlled by design. For the simulations of the system, we employ the Light-DMRG algorithm²¹, see Methods.

The model. The many body Hamiltonian of the system rotating at frequency ω_p , following analog atomic systems methods^{22,23} is:

$$\mathcal{H} = -\hbar\Delta_c\hat{a}^\dagger\hat{a} + \hbar\omega_0\sum_n\hat{S}_n^z + \hbar J\sum_n\hat{S}_n^z\hat{S}_{n+1}^z + \frac{\hbar V_p}{\sqrt{N}}(\hat{a}^\dagger + \hat{a})\sum_n J_n^{pc}\hat{S}_n^x \quad (1)$$

where the first term is the energy of the cavity photons, $\Delta_c = \omega_p - \omega_c$ is the cavity detuning, \hbar the reduced Planck constant, $\hat{a}^{(\dagger)}$ is the cavity mode photonic annihilation (creation) operator. The energy of each spin $1/2$ is $\hbar\omega_0$, the interaction between spins in the absence of cavity light is given by the Ising Hamiltonian with $\hbar J$ the energy of the exchange of spins. The interaction between the photons and the spins is given in the typical Dicke form^{1,11,24} with $\hbar V_p$ the effective pump potential, the overlap amplitudes of the spins with the pump and cavity light are given by $J_n^{pc} = \cos(\pi n)\cos(\pi n\cos\phi)$ at each localized spin with site n and N spins; the angle between the pump wave vector $\mathbf{k}_p = |\mathbf{k}_p|\hat{e}_p$ and the cavity wavevector $\mathbf{k}_c = |\mathbf{k}_c|\hat{e}_c$ is ϕ , the spins are along \hat{e}_x as shown in Fig.1, see Methods. Similar to atomic systems²⁻⁴, we consider three different configurations depending on the light induced emergent coupling of the spins due to the cavity field, for $\phi = 0$ the coupling is homogenous across the lattice inducing a single mode, with $\phi = \pi/2$ we induce a two mode staggered ordering with couplings $J_n^{pc} = (-1)^n$ and with $\phi = \arccos(1/5) \approx$

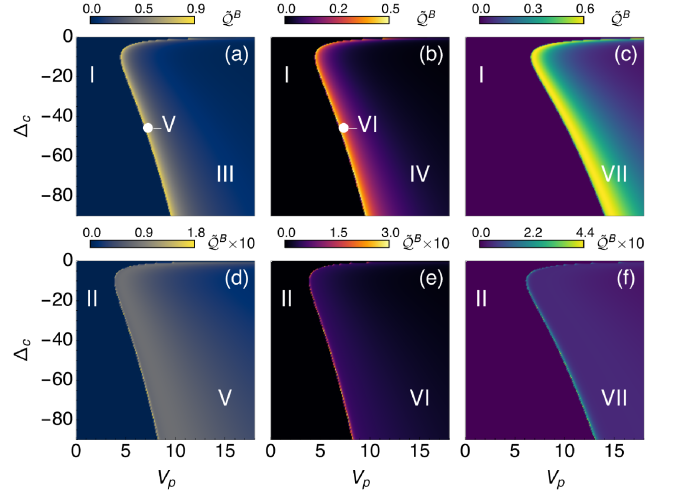


FIG. 2. **Phase diagrams for different light induced mode structures and the behavior of the mean bond-nematic order parameter (\tilde{Q}^B).** When the system becomes superradiant and the quantization axis of the spins changes there is the formation of bond nematic quantum states. These can persist deeper into the superradiant state depending on the short-range spin interaction strength J and the light induced configuration. Panels (a,b,c): correspond to $J < 0$, normal FM state (I) and superradiant configurations (III-VII). Panels (d,e,f): correspond to $J > 0$ normal AFM state (II) and superradiant configurations (V-VII). The light induced mode structures are: (a,d) for $\phi = 0$ diffraction maxima [●●], (b,e) for $\phi = \pi/2$ diffraction minima [●●] and (c,f) for $\phi = \arccos(1/5)$, the golden ratio configuration [●●●●], as shown in Fig.1 (a). The order parameters of different phases are in Table I. Parameters in the simulations are: $N = 400$ spins, $\omega_0/|J| = 0.1$, $\kappa/|J| = 10$ with Δ_c and V_p in units of $|J|$.

0.436π , the golden ratio mode, we induce a pattern for the couplings $J_n^{pc} = \{-\varphi/2, (\varphi-1)/2, (\varphi-1)/2, -\varphi/2, 1\}$ every 5 sites with $\varphi \approx 1.61803$ the golden ratio.

The order parameters. In spin systems one body order parameters that characterize the magnetic ordering in the system are the magnetizations $\mathcal{M}_0^\nu = \sum_n \cos(\theta n)\langle \hat{S}_n^\nu \rangle / N$, with $\nu \in \{x, y, z\}$ and $\theta = 0$ for the magnetization (FM ordering) or $\theta = \pi$ the staggered magnetization (AFM ordering) in the spin axis α . Considering genuine many body spin quantum correlations, for spin $1/2$ systems the traceless bond nematic tensor of rank 2 is defined as:

$$\mathcal{Q}_{nm}^{\nu\eta} = \langle \hat{S}_n^\nu \hat{S}_m^\eta + \hat{S}_n^\eta \hat{S}_m^\nu \rangle (1 - \delta_{\nu\eta})(1 - \delta_{nm}) / 2 \quad (2)$$

for each pair of sites nm , with $\nu, \eta \in \{x, y, z\}$. This tensor measures the quadrupolar deformations in the system between different sites as the on-site signal is trivial for spin $1/2$ systems^{25,26}. The bond nematic order parameter for each pair of sites nm is the largest eigenvalue of

the tensor such that $Q_{nm}^B = \max(\text{Sp}(Q_{nm}))$. It is useful to define the average over all the pairs of sites in the lattice as the global order parameter of how nematic is the state. Thus, we define the mean bond nematic order parameter as $\tilde{Q}^B = \sum_{nm} Q_{nm}^B / N^2$, this is shown in Fig.2 for the different light induced modes in Fig.1 and different Ising couplings (FM/AFM). Due to the “ x - z ” symmetry of \mathcal{H} , the nematic order is uniaxial with $Q_{nm}^B = |Q_{nm}^{xz}| \neq 0$ whenever it emerges. Clearly, this is an effect that cannot be obtained by mean-field calculations and it clarifies the underlying mechanism that triggers the quantum phase transition due to strong quantum correlations. In addition to the nematic character of the states, it is well known that magnon pair states can be supported with nematic ordering^{25,27}, the magnon pairs at different sites are characterized by pair amplitude $\mathcal{P}_{nm} = \langle \hat{S}_n^- \hat{S}_m^- \rangle = \langle \hat{S}_n^x \hat{S}_m^x - \hat{S}_n^y \hat{S}_m^y - i \hat{S}_n^x \hat{S}_m^y - i \hat{S}_n^y \hat{S}_m^x \rangle$ and the global magnon pair order parameter can be defined as $\tilde{\mathcal{P}} = \sum_{nm} |\mathcal{P}_{nm}| / N^2$.

Quantum phases. We find a rich set of scenarios that can be tailored depending on the geometry of the light and the short range Ising interaction present either FM _{z} or AFM _{z} . The underlying Ising interaction determines how the correlations induced by the cavity light form the SR phases in the system that can be FM _{x} /AFM _{x} with [Fig.2 (a,d)/(b,e)] and without nematic character of fully nematic with FM _{φ} pattern [Fig.2 (c,f)] in the system. All the phases present are shown in Fig.2 and the Table I has the definitions and behavior of the order parameters for each quantum phase, further details can be found in the Supplemental Material. We find that as the cavity light emerges, the spins twist their quantization axis leading to the formation of a uniaxial quantum spin nematic²⁸ as the clear signature of the quantum phase transition. Moreover, the presence of these states can be stabilized beyond the transition region in the φ induced spin modes in both underlying short range FM _{z} and AFM _{z} couplings Fig. 2 (c,f). From our simulations, we find that FM _{z} Ising interactions are better for the stabilization of bond nematic order. Intuitively, this can be understood as the rigidity of the underlying FM _{z} state is stronger with respect to the twist applied to the spin quantization axis by the cavity light with respect to the AFM _{z} state that is already minimizing the total spin in the system in the normal state. The quantum phase transitions in the set are strongly dependent on the light and cavity parameters with qualitative similar features that allow to explore depending on the cavity detuning and the pump strength how the quantum phase transitions take place in a single setup. Surprisingly, we find that all the SR states support long range magnon pairs, even with a minimal display ($Q^B \approx 0 \neq 0$) of nematic order. Measuring the cavity light amplitude $|\langle \hat{a} \rangle|$, the magnetizations and the spin correlations it is experimentally viable to reconstruct the phase diagrams of Fig. 2. In similar setups, these are routinely produced experimentally¹. For addi-

tional details on all the observables see the Supplemental Material.

Local observables and entanglement measures. Beyond one (FM _{x}) and two (AFM _{x}) cavity induced modes, the φ setup stabilizes entirely the bond nematic state. In Fig. 3, we can see the local structure of Q_{nm}^B and \mathcal{P}_{nm} in the middle of the chain across all the other spins for (a,c) with $J > 0$ and (b,d) with $J < 0$. This illustrates the long range structured character of both the magnon pairing and the nematic order in the system, that presents well defined amplitude oscillations across the whole chain similar to frustrated systems²⁵. As non-trivial many body quantum correlations are present in the system, we analyze how entanglement behaves in the system using the entanglement entropy \mathcal{S}_E considering different subsets of sites in the chain, see the insets of Fig.3. In contrast to the strength of the Q_{nm}^B , the maximum \mathcal{S}_E is larger for AFM _{z} coupling as it favors the production of singlets than for the FM _{z} , for all partitions. In (a.1,b.1), we show the entanglement of each of the 3 modes (R,B,G) across the whole lattice induced by the φ setting and in (c.1,d.1) the entanglement of the groups of spin singlets embedded in the mode structure. Clearly, the components that form the singlets are more entangled and the singlets themselves have high entanglement, with respect to the G mode. Indeed, this light-matter system acts like a collective entanglement gate protocol naturally and efficiently. The behavior across the transition of these modes allows for a useful qubit resource that in principle could be exploited tuning the light pumped into the system via V_p and Δ_c . Note that this is only possible due to the fact that the SR modes compete with the short range Ising background twisting the quantization of the spins due to emergent quadrupolar coupling between different sites across the chain. In the absence of the Ising interaction or the cavity coupling the entanglement is minimal and fragile between the spins.

In conclusion, we have found a path towards an efficient mechanism to generate highly entangled spin structures embedded in spin chains due to cavity light and its combination with short range processes. Moreover, we have identified that this can be controlled by the geometry of light pumped into the system. It is possible to induce different concentrations of light induced modes by choosing the angle between the cavity axis and the pumped light as $\phi = \arccos(1/(2M - 1))$ with M integer, this choice will generate M modes with non-zero couplings induced by light across the system. The key ingredient to achieve this entanglement resource is the emergence of bond nematic order in the system due to the anharmonic response of the spins embedded in the chain. Spin quantum correlations drive the quantum phase transition to the SR state with the emergence of magnon pairs. In principle, these magnon pairs could be used as another source to manipulate information across the chain. We have extended our previous devel-

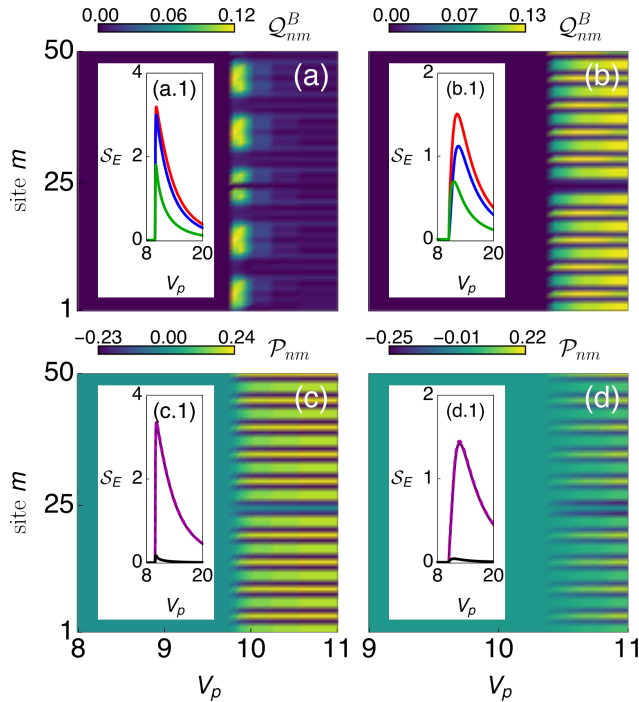


FIG. 3. **Behavior with the golden ratio mode φ induced by light. Main Panels: Local bond nematic order parameter Q_{nm}^B , local magnon pair amplitude P_{nm} . Inset Panels: Entanglement entropies S_E for different mode structures in the system.** Main panels (a,b) show the amplitude variation of Q_{nm}^B near the transition to the SR state and how long range structured correlations emerge across the whole lattice. Main panels (c,d) show the amplitude variation of the magnon pairs with long range coherent oscillations in the SR. The Ising coupling is $J > 0$ for (a, c) and $J < 0$ for (b, d). Inset panels (a.1,b.1) show the entanglement entropy of the sites with R modes (red; [● - - ● -]), the B modes (blue) [- ● ● -], and the G mode (green) [- - ●], across the whole lattice, following Fig.1. Inset panels (c.1,d.1) show the entanglement entropy of the sites AFM_x singlet sites (1 + k and 2 + k) [solid purple, ● ● - -] and (3 + k and 4 + k) [dashed purple, - - ● ● -] across the whole lattice with $k = 5 \times (n - 1)$, $n = 1, \dots, N/5$; the entanglement entropy of half the chain is shown in black. The parameters are: $n = 25$ the middle of the chain for Q_{nm}^B and P_{nm} ; $N = 50$ sites, $\omega_0/|J| = 0.1$, $\kappa/|J| = 10$ with Δ_c and V_p in units of $|J|$ for all plots.

opments with Light-matter DMRG and applied the technique to analyze spin systems opening an efficient pathway towards the simulation of these light-matter systems that efficiently captures the quantum correlated nature of spin systems. Notably our work could be used for the optimization entanglement properties in the design of wave guides for analog ion systems. Our methods allow the inclusion of quantum correlated effects beyond

mean field schemes in analog qubit systems of arrays of ions^{17,18}, neutral atoms^{14,29}, Rydberg atoms^{15,16}, ultracold fermions³⁰ and possibly arrays of giant atoms³¹

We thank the hospitality of J. Hoffmann of the Physics Department of the University of Gothenburg and the Theoretical Physics Seminar where these ideas were first exposed. We thank H. Ritsch, T. Donner, F. Mivehvar, A. Frisk and A. Bautista-Salvador for useful discussions. This work is partially supported by the grants UNAM-DGAPA-PAPIIT: IN118823, UNAM-DGAPA-PAPIIT: IG101826, UNAM-CIC: Apoyo a Laboratorios Nacionales 2025, CONAHCYT/SECIHITI: LNC-2023-51, as well as by grants from NVIDIA and utilized NVIDIA RTX 6000 Ada.

METHODS

Due to the different time scales of the spin and the cavity field dynamics, one can adiabatically eliminate the latter similar to atomic systems¹. If the energy scales are not that separated the scheme can be amended by considering additional contributions as in²³. The photonic operator \hat{a} is replaced by its steady state value $\alpha = \langle \hat{a} \rangle$. This is found taking the steady state value from the Heisenberg equation of motion for the light field: $d\langle \hat{a} \rangle / dt = (i/\hbar) \langle [\mathcal{H}, \hat{a}] \rangle - \kappa \langle \hat{a} \rangle = 0$. Here the dissipation from the cavity is introduced phenomenologically through the cavity decay rate κ . It follows that,

$$\alpha = \frac{\hbar V_p}{(\hbar \Delta_c + i \hbar \kappa) \sqrt{N}} \sum_n J_n^{pc} \langle \hat{S}_n^x \rangle \quad (3)$$

which is solved self consistently as function of V_p , Δ_c and κ . Note that in the SR state the phase of the light field is π in this setup. Following³², the overlap integrals J_i^{pc} can be written in terms of the incident pump field, the overlap with the cavity mode and the localized spins at position n as,

$$J_n^{pc} = \int dx |w(x - x_n)|^2 \cos(\mathbf{k}_p \cdot \mathbf{x}) \cos(\mathbf{k}_c \cdot \mathbf{x}) \quad (4)$$

$$\approx \cos(\pi n) \cos(\pi n \cos \phi) \quad (5)$$

with $w(x)$ the effective Wannier function that describes the localization of the each spin at position x , with ϕ the angle between the cavity axis and the pump wavevector. Note that the pump, the cavity mode and the spins positions have been chosen commensurate to each other fixing $|\mathbf{k}_p| = |\mathbf{k}_c| = 2\pi/\lambda$ with the lattice spacing between spins as $a = \lambda/2$ and $x_n = na$.

Self Consistent Algorithm: light-matter DMRG for spins

Similar to the light-matter DMRG algorithm for ultracold atoms²¹ we employ the same structure for the spin

system, a key difference here is that the Wannier functions have been approximated static (not dependent on the cavity light) without loss of generality, further refinements for higher dimensions can be implemented as well as the full dependence on cavity light. The phase diagrams are obtained solving (3) self consistently. We start giving an ansatz $\alpha \neq 0$, we obtain the ground state of \mathcal{H} substituting $\hat{a} \rightarrow \alpha$ and $\hat{a}^\dagger \rightarrow \alpha^*$. Then we obtain a new value for α from (3). This cycle is repeated until convergence is achieved with a tolerance less than single precision. There can be multiple solutions for α for fixed V_p , Δ_c and κ , so it is necessary to keep only the lowest energy state.

To find the effective ground state of (1) for a fixed parameter set in the self-consistent loop, we perform simulations using DMRG^{33,34} with the aid of the ITensor library³⁵. We simulate a 1D chain with 400 sites with open boundary conditions; we verified lower number of sites recover qualitative similar results.

* scaballero@fisica.unam.mx

1. Mivehvar, F., Piazza, F., Donner, T. & Ritsch, H. Cavity qed with quantum gases: new paradigms in many-body physics. *Advances in Physics* **70**, 1–153 (2021). URL <https://doi.org/10.1080/00018732.2021.1969727>.
2. Elliott, T. J., Kozłowski, W., Caballero-Benitez, S. F. & Mekhov, I. B. Multipartite entangled spatial modes of ultracold atoms generated and controlled by quantum measurement. *Phys. Rev. Lett.* **114**, 113604 (2015). URL <https://link.aps.org/doi/10.1103/PhysRevLett.114.113604>.
3. Mazzucchi, G., Kozłowski, W., Caballero-Benitez, S. F., Elliott, T. J. & Mekhov, I. B. Quantum measurement-induced dynamics of many-body ultracold bosonic and fermionic systems in optical lattices. *Phys. Rev. A* **93**, 023632 (2016). URL <https://link.aps.org/doi/10.1103/PhysRevA.93.023632>.
4. Caballero-Benitez, S. F. & Mekhov, I. B. Quantum optical lattices for emergent many-body phases of ultracold atoms. *Phys. Rev. Lett.* **115**, 243604 (2015). URL <https://link.aps.org/doi/10.1103/PhysRevLett.115.243604>.
5. Baumann, K., Guerlin, C., Brennecke, F. & Esslinger, T. Dicke quantum phase transition with a superfluid gas in an optical cavity. *Nature* **464**, 1301–1306 (2010). URL <https://doi.org/10.1038/nature09009>.
6. Li, X. *et al.* First order phase transition between two centro-symmetric superradiant crystals. *Phys. Rev. Res.* **3**, L012024 (2021). URL <https://link.aps.org/doi/10.1103/PhysRevResearch.3.L012024>.
7. Sachdev, S. *Quantum Phase Transitions* (Cambridge University Press, 2011), 2 edn.
8. Landig, R. *et al.* Quantum phases from competing short- and long-range interactions in an optical lattice. *Nature* **532**, 476–479 (2016). URL <https://doi.org/10.1038/nature17409>.
9. Klinder, J., Keßler, H., Reza Bakhtiari, M., Thorwart, M. & Hemmerich, A. Observation of a superradiant mott insulator in the dicke-hubbard models. *Phys. Rev. Lett.* **115**, 230403 (2015). URL <https://journals.aps.org/prl/pdf/10.1103/PhysRevLett.115.230403>.
10. Léonard, J., Morales, A., Zupancic, P., Esslinger, T. & Donner, T. Supersolid formation in a quantum gas breaking a continuous translational symmetry. *Nature* **543**, 87–90 (2017). URL <https://doi.org/10.1038/nature21067>.
11. Kroeze, R. M., Guo, Y., Vaidya, V. D., Keeling, J. & Lev, B. L. Spinor self-ordering of a quantum gas in a cavity. *Phys. Rev. Lett.* **121**, 163601 (2018). URL <https://link.aps.org/doi/10.1103/PhysRevLett.121.163601>.
12. Lozano-Méndez, K., Cásares, A. H. & Caballero-Benítez, S. F. Spin entanglement and magnetic competition via long-range interactions in spinor quantum optical lattices. *Phys. Rev. Lett.* **128**, 080601 (2022). URL <https://link.aps.org/doi/10.1103/PhysRevLett.128.080601>.
13. Ríos-Sánchez, B. & Caballero-Benítez, S. F. Control, competition and coexistence of effective magnetic orders by interactions in bose-einstein condensates with high-q cavities. *New J. Phys.* **27**, 113203 (2025). URL <https://iopscience.iop.org/article/10.1088/1367-2630/ae1b32>.
14. Song, E. Y. *et al.* A dissipation-induced superradiant transition in a strontium cavity-qed system. *Science Advances* **11**, eadu5799 (2025). URL <https://www.science.org/doi/abs/10.1126/sciadv.adu5799>. <https://www.science.org/doi/pdf/10.1126/sciadv.adu5799>.
15. Yasir, K. A. & Liu, W.-M. *Rydberg Atoms in Cavity* (Springer Nature, Singapore, 2026), 1 edn.
16. De Santis, J. *et al.* Realization of a cavity-coupled rydberg array (2026). URL <https://doi.org/10.48550/arXiv.2602.12152>. 2602.12152.
17. Srinivas, R. *et al.* Trapped-ion spin-motion coupling with microwaves and a near-motional oscillating magnetic field gradient. *Phys. Rev. Lett.* **122**, 163201 (2019). URL <https://link.aps.org/doi/10.1103/PhysRevLett.122.163201>.
18. Zarantonello, G. *et al.* Robust and resource-efficient microwave near-field entangling $^9\text{be}^+$ gate. *Phys. Rev. Lett.* **123**, 260503 (2019). URL <https://link.aps.org/doi/10.1103/PhysRevLett.123.260503>.
19. Alvarez-Giron, W., Solano, P., Sinha, K. & Barberis-Blostein, P. Delay-induced spontaneous dark-state generation from two distant excited atoms. *Phys. Rev. Res.* **6**, 023213 (2024). URL <https://link.aps.org/doi/10.1103/PhysRevResearch.6.023213>.
20. Solano, P., Barberis-Blostein, P., Fatemi, F. K., Orozco, L. A. & Rolston, S. L. Super-radiance reveals infinite-range dipole interactions through a nanofiber. *Nature Communications* **8**, 1857 (2017). URL <https://doi.org/10.1038/s41467-017-01994-3>.
21. Ramírez-Barajas, A. U. & Caballero-Benitez, S. F. Structural dynamics and strong correlations in dynamical quantum optical lattices. *Phys. Rev. Lett.* **135**, 120602 (2025). URL <https://link.aps.org/doi/10.1103/gvm2-b46t>.
22. Maschler, C., Mekhov, I. B. & Ritsch, H. Ultracold atoms in optical lattices generated by quantized light fields. *The European Physical Journal D* **46**, 545–560 (2008). URL <https://doi.org/10.1140/epjd/e2008-00016-4>.
23. Caballero-Benitez, S. F. & Mekhov, I. B. Quantum properties of light scattered from structured many-body phases of ultracold atoms in quantum optical lattices. *New J. Phys.* **17**, 123023 (2015). URL <https://iopscience.iop.org/article/10.1088/1367-2630/17/12/123023>.

24. Morales, A. *et al.* Two-mode dicke model from non-degenerate polarization modes. *Phys. Rev. A* **100**, 013816 (2019). URL <https://link.aps.org/doi/10.1103/PhysRevA.100.013816>.
25. Shannon, N., Momoi, T. & Sindzingre, P. Nematic order in square lattice frustrated ferromagnets. *Phys. Rev. Lett.* **96**, 027213 (2006). URL <https://link.aps.org/doi/10.1103/PhysRevLett.96.027213>.
26. Jiang, S., Romhányi, J., White, S. R., Zhitomirsky, M. E. & Chernyshev, A. L. Where is the quantum spin nematic? *Phys. Rev. Lett.* **130**, 116701 (2023). URL <https://link.aps.org/doi/10.1103/PhysRevLett.130.116701>.
27. Chubukov, A. V. Chiral, nematic, and dimer states in quantum spin chains. *Phys. Rev. B* **44**, 4693–4696 (1991). URL <https://link.aps.org/doi/10.1103/PhysRevB.44.4693>.
28. Chojnacki, L., Pohle, R., Yan, H., Akagi, Y. & Shannon, N. Gravitational wave analogs in spin nematics and cold atoms. *Phys. Rev. B* **109**, L220407 (2024). URL <https://link.aps.org/doi/10.1103/PhysRevB.109.L220407>.
29. Cooper, E. S., Kunkel, P., Periwal, A. & Schleier-Smith, M. Graph states of atomic ensembles engineered by photon-mediated entanglement. *Nature Physics* **20**, 770–775 (2024). URL <https://doi.org/10.1038/s41567-024-02407-1>.
30. Helson, V. *et al.* Density-wave ordering in a unitary fermi gas with photon-mediated interactions. *Nature* **618**, 716–720 (2023). URL <https://doi.org/10.1038/s41586-023-06018-3>.
31. Chen, G. & Frisk Kockrum, A. Scalable quantum simulator with an extended gate set in giant atoms. *Quantum* **10**, 1992 (2026). URL <https://doi.org/10.22331/q-2026-01-30-1992>.
32. Kozłowski, W., Caballero-Benitez, S. F. & Mekhov, I. B. Probing matter-field and atom-number correlations in optical lattices by global nondestructive addressing. *Phys. Rev. A* **92**, 013613 (2015). URL <https://link.aps.org/doi/10.1103/PhysRevA.92.013613>.
33. White, S. R. Density matrix formulation for quantum renormalization groups. *Phys. Rev. Lett.* **69**, 2863–2866 (1992). URL <https://link.aps.org/doi/10.1103/PhysRevLett.69.2863>.
34. Schollwöck, U. The density-matrix renormalization group. *Rev. Mod. Phys.* **77**, 259 (2005). URL <https://journals.aps.org/rmp/abstract/10.1103/RevModPhys.77.259>.
35. Fishman, M., White, S. R. & Stoudenmire, E. M. Codebase release 0.3 for ITensor. *SciPost Phys. Codebases* 4–r0.3 (2022). URL <https://scipost.org/10.21468/SciPostPhysCodeb.4-r0.3>.

Supplemental material for: Quantum Correlations and Entanglement in Generalized Dicke-Ising Models

Santiago F. Caballero-Benitez¹

¹Instituto de Física, LSCSC-LANMAC, Universidad Nacional Autónoma de México, Ciudad de México 04510, Mexico

ORDER PARAMETERS FOR DIFFERENT SETUPS

In Fig. S1 we show the behavior of the order parameters for $J < 1$ and $\phi = 0$. In Fig. S2 we show the behavior of the order parameters for $J > 1$ and $\phi = 0$. In Fig. S3 we show the behavior of the order parameters for $J < 1$ and $\phi = \pi/2$. In Fig. S4 we show the behavior of the order parameters for $J > 1$ and $\phi = \pi/2$. In Fig. S5 we show the behavior of the order parameters for $J < 1$ and $\phi = \arccos(1/5)$. In Fig. S6 we show the behavior of the order parameters for $J > 1$ and $\phi = \arccos(1/5)$. In Fig. S7 we show the behavior of the entanglement across the half the chain corresponding to Fig. 2. The parameters in all plots are $N = 400$ sites with open boundary conditions using light-matter DMRG, $\omega/|J| = 0.1$, $\kappa/|J| = 10$, with Δ_c and V_p in units of $|J|$. Only the non-trivial order parameters are displayed for each setup.

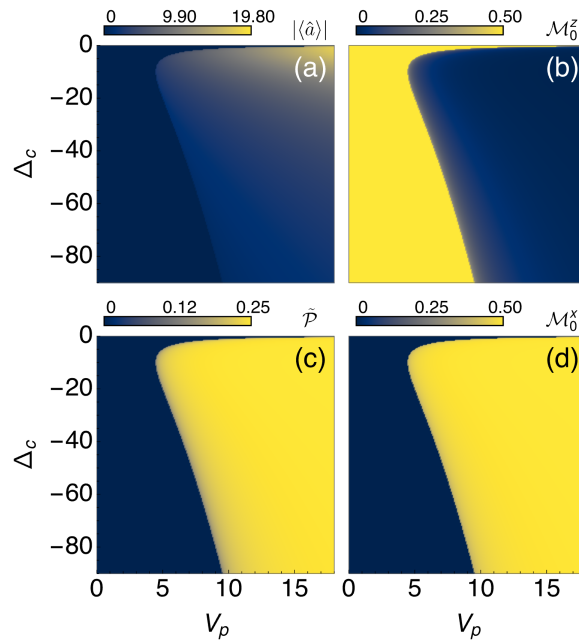


FIG. S1. **Order parameters for normal Ferromagnetic ordering and Superradiant Ferromagnetic setup.** (a) Cavity light, (b) magnetization along quantization axis “z”, (c) mean magnon pairing amplitude, (d) magnetization along quantization axis “x”. The Ising coupling is $J < 0$ FM.

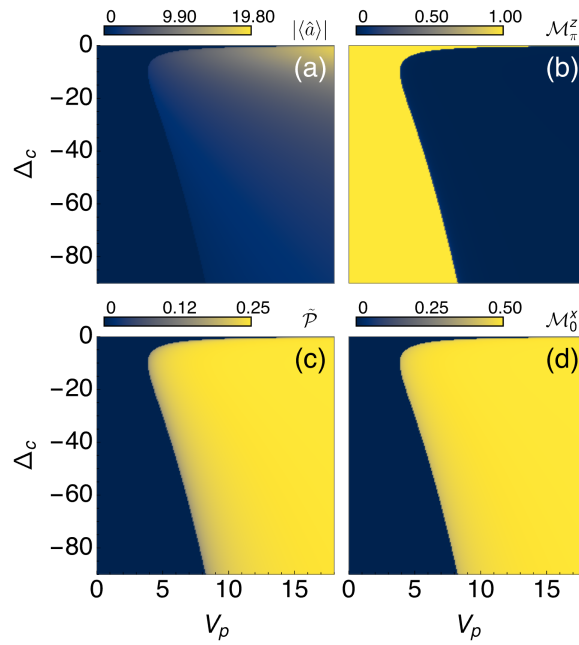


FIG. S2. **Order parameters for normal Anti-ferromagnetic ordering and Superradiant Ferromagnetic setup.** (a) Cavity light, (b) staggered magnetization along quantization axis “z”, (c) mean magnon pairing amplitude, (d) magnetization along quantization axis “x”. The Ising coupling is $J > 0$ AFM.

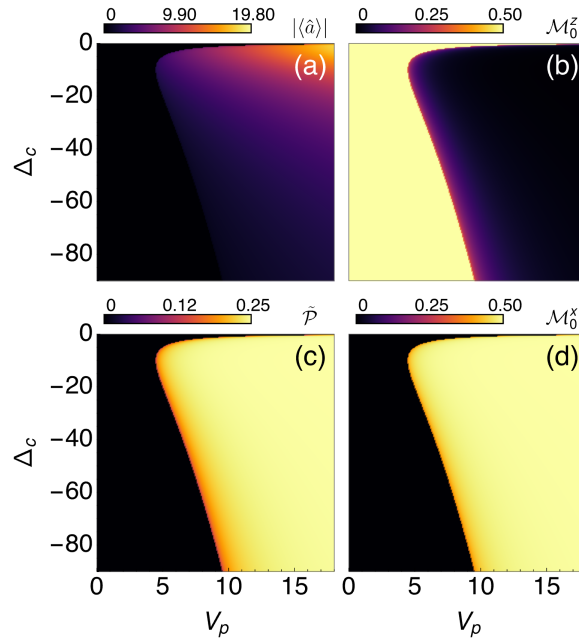


FIG. S3. **Order parameters for normal Ferromagnetic ordering and Superradiant Anti-ferromagnetic setup.** (a) Cavity light, (b) magnetization along quantization axis “z”, (c) mean magnon pairing amplitude, (d) magnetization along quantization axis “x”. The Ising coupling is $J > 0$ AFM.

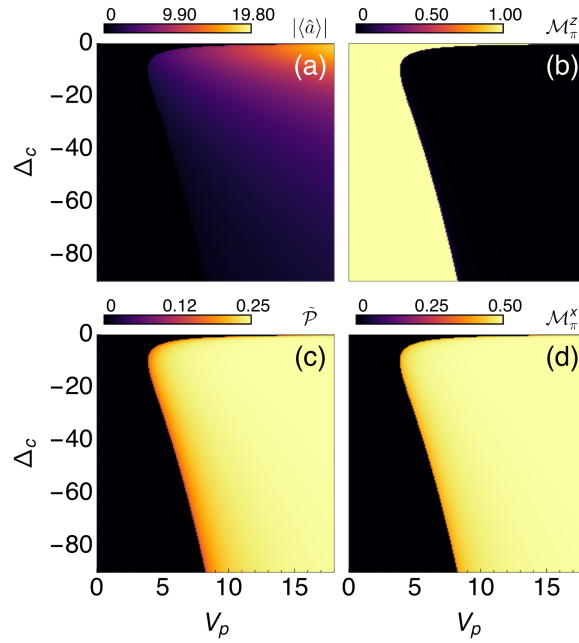


FIG. S4. **Order parameters for normal Anti-ferromagnetic ordering and Superradiant Anti-ferromagnetic setup.** (a) Cavity light, (b) staggered magnetization along quantization axis “z”, (c) mean magnon pairing amplitude, (d) staggered magnetization along quantization axis “x”. The Ising coupling is $J > 0$ AFM.

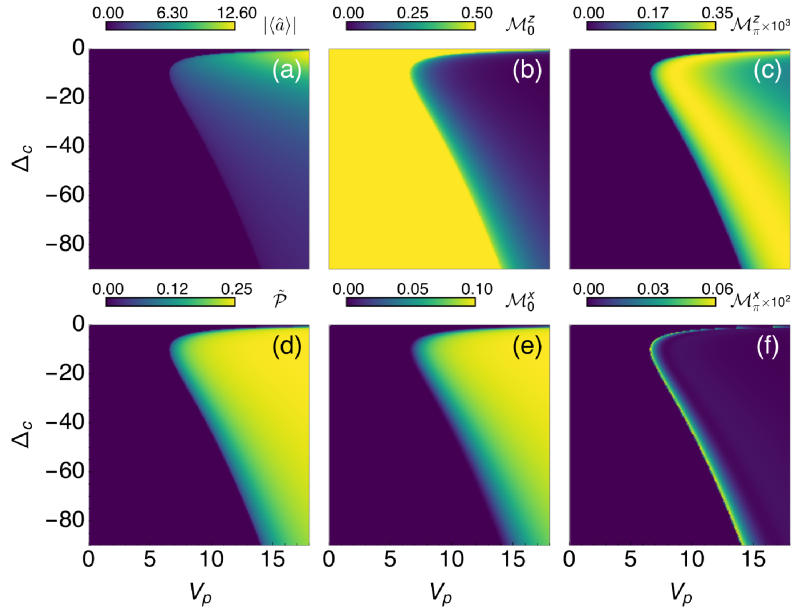


FIG. S5. **Order parameters for normal Ferromagnetic ordering and Superradiant Bond-nematic setup.** (a) Cavity light, (b) magnetization along quantization axis “z”, (c) staggered magnetization along quantization axis “z”, (d) mean magnon pairing amplitude, (e) magnetization along quantization axis “x”, (e) staggered magnetization along quantization axis “x”. The Ising coupling is $J < 0$ FM.

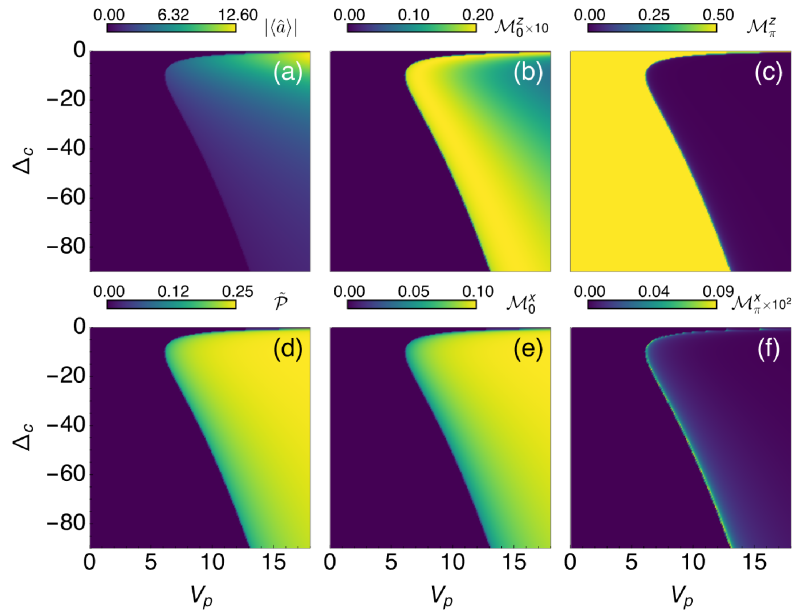


FIG. S6. **Order parameters for normal Anti-ferromagnetic ordering and Superradiant Bond-nematic setup.** (a) Cavity light, (b) magnetization along quantization axis “z”, (c) staggered magnetization along quantization axis “z”, (d) mean magnon pairing amplitude, (e) magnetization along quantization axis “x”, (f) staggered magnetization along quantization axis “x”. The Ising coupling is $J > 0$ AFM.

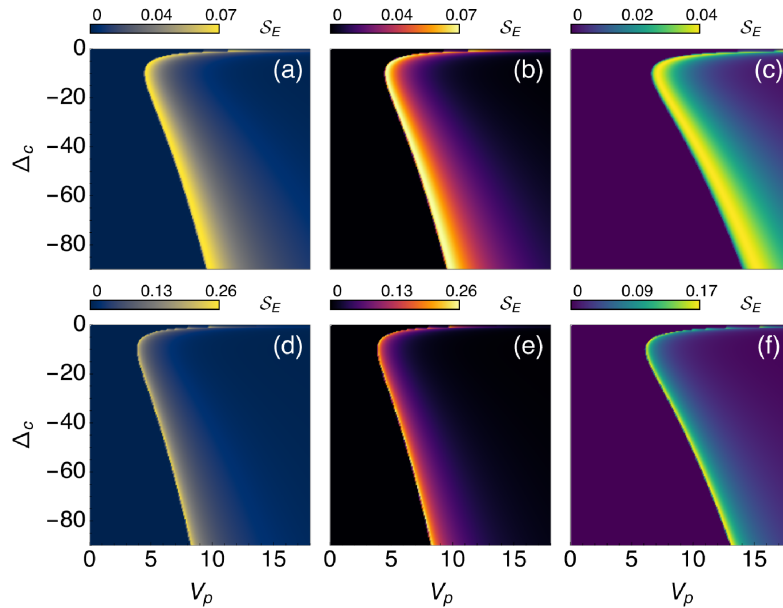


FIG. S7. **Entanglement entropy across half the chain for different configurations.** The Entanglement entropy corresponds to the setups in Fig. 2. As the SR transition is approached entanglement is maximal. Parameters are: (a) $J < 1$, $\phi = 0$; (b) $J < 1$, $\phi = \pi/2$; (c) $J < 1$, $\phi = \arccos(1/5)$; (d) $J > 1$, $\phi = 0$; (e) $J > 1$, $\phi = \pi/2$; (f) $J > 1$, $\phi = \arccos(1/5)$;